Landsc Ecol (2025) 40:27
https://doi.org/10.1007/s10980-024-02031-7

RESEARCH ARTICLE

Estimation of leaf area index in sagebrush steppe with low cost unoccupied aerial systems

Craig D. Woodruff · Patrick E. Clark · Peter J. Olsoy · Josh Enterkine

Received: 23 September 2024 / Accepted: 23 December 2024

Abstract

Context Leaf area index (LAI) strongly influences the carbon and water cycle in drylands, but accurate estimation of LAI relies on field methods that are expensive and time intensive. Very high-resolution imagery from unoccupied aerial systems (UAS) offers a potential solution for monitoring LAI, but estimation methods derived from cost effective red, green, and blue (RGB) sensors are untested in these semi-arid ecosystems.

Objectives The objective of our study was to test whether LAI could be estimated with very high resolution UAS collected RGB and canopy height data. Additionally, we sought to validate the model accuracy at the plot (1 m^2) scale, test the accuracy at the macroplot (1 ha) scale, and assess the within plot impact of shadows.

Methods We used a Random Forest machine learning model to estimate LAI in a Wyoming big sagebrush community in the Reynolds Creek Experimental Watershed using high resolution (< 1 cm^2) UAS imagery collected in 2021 as predictors and plot scale point intercept (quadrat design) field data as the LAI reference.

Results Random Forest modeled estimates of LAI were accurate at the plot ($r^2 = 0.69$, MAE = 0.08, RMSE = 0.10), and the macroplot scales (error of 0.065), and mean within plot shadow error was 0.06.

Conclusions This research demonstrates high resolution UAS data can rapidly and accurately estimate LAI, with a limited number of field measurements, potentially allowing land managers to survey seasonally and spatially heterogeneous LAI 1 hectare at a time over the vast rangelands in the Great Basin and similar ecosystems worldwide.

Keywords UAS · Leaf area index · Rangelands · Random forest · Machine learning

C. D. Woodruff (✉) · P. E. Clark
Northwest Watershed Research Center, USDA Agricultural Research Service, 251 E Front Street, Suite 400, Boise, ID 83702, USA
e-mail: craig.woodruff@usda.gov

P. J. Olsoy
USDA Agricultural Research Service, Range and Meadow Forage Management Research, 67826A OR-205, Burns, OR 97720, USA

J. Enterkine
Department of Geosciences, Boise State University, 1910 W University Dr, Boise, ID 83725, USA

Introduction

Leaf area index (LAI) is the green leaf unit area per unit area (m^2/m^2) that intercepts light and is a critical parameter in global models of water and carbon dynamics (Bonan 1993; Hao et al. 2018; Hoek Van Dijke et al. 2020; Pan et al. 2021). Quantifying LAI in dryland ecosystems is important because these

Published online: 22 January 2025

ecosystems represent about 60 million km^2, or 41%, of the Earth's terrestrial surface (Safriel and Adeel 2005; Prăvălie 2016). LAI variability in dryland ecosystems is driven by the spatial heterogeneity of plant functional types, fractional cover, canopy structure, water availability to support transpiration, seasonal dynamics of each vegetation type, and climate variability (Mougin et al. 2014; Bonan 2016; Taylor et al. 2021; MacBean et al. 2021; Chen et al. 2023). Measuring or estimating LAI with field techniques or local instrumentation is costly and does not adequately sample the scope and diversity of spatially extensive and complex dryland ecosystems.

Methods to accurately measure and estimate LAI are time consuming and sometimes unreliable. Destructive harvest of photosynthetic matter is considered the most reliable, but has significant setbacks including labor intensive sampling, sample loss and degradation in storage, and errors associated with proper photo-scanning of the samples (Beerling and Fry 1990; Bonham 2013). Instrumentation like Photosynthetically Active Radiation (PAR) sensors are a rapid collection alternative, but fail to differentiate photosynthetic from non-photosynthetic material leading to overestimation in woody shrub systems like sagebrush (Finzel et al. 2012). Terrestrial laser scanning in the visible and near infrared spectral range can accurately distinguish photosynthetic and non-photosynthetic material, but careful consideration must be taken to include multiple view angles ultimately reducing sampling time efficiency (Olsoy et al. 2016). Point intercept sampling is an accurate method to estimate LAI, but accuracy varies by growth form and data collection is labor intensive and difficult over large spatial scales (Clark and Seyfried 2001). Field methods often fail to representatively sample the heterogeneous landscapes of drylands, a problem potentially addressed by aerial remote sensing systems.

Satellite remote sensing offers broad spatial coverage and repeated retrieval of LAI through direct relationships like the Normalized Difference Vegetation Index (NDVI) (Fan et al. 2009), Simple Ratio (Chen 1996), and the Normalized Difference Red-Edge (NDRE) (Delegido et al. 2013). However, the spatial resolution of many satellites is too coarse to capture the heterogeneity of sagebrush (*Artemisia* spp.)-dominated rangelands, a type of dryland ecosystem. Furthermore, the large woody component in sagebrush-dominated rangelands, leads to overestimation of LAI with satellite remote sensing (Hunt, Jr. et al. 2003). Methods have been developed to increase the LAI estimation spatial resolution (500 m) of the Moderate Resolution Imaging Spectroradiometer (MODIS) down to 10 m with data fusion (Wang et al. 2019), but remotely sensed data products can exhibit large variability as spatial resolutions change, calling into question the reliability of these estimates (Liu et al. 2018). The variability in LAI may be due to the subtle vegetation dynamics or "mixed pixels" characteristic of rangelands and even at 10-m spatial resolution these dynamics may need to be represented with fuzzy classifications (Enterkine et al. 2024). A finer spatial resolution may help to increase the reliability of remotely sensed LAI estimates, but it is unknown what spatial resolution is needed.

Unmanned aerial system (UAS) remote sensing can rapidly collect very high spatial resolution (< 1 cm^2) imagery and has the potential to increase LAI estimation accuracy while maintaining broad spatial coverage. UAS-based LAI estimation has been demonstrated in cropping systems including maize (Peng et al. 2021; Du et al. 2022; Buthelezi et al. 2023), winter wheat (Hasan et al. 2019; Wittstruck et al. 2022; Wang et al. 2022), rice (Gong et al. 2021), onions (Córcoles et al. 2013), vineyards (Kalisperakis et al. 2015; Comba et al. 2020), kiwi fruit (Zhang et al. 2022), coffee (Mendes Dos Santos et al. 2020), and apples (Liu et al. 2021). In all these studies, the cropping systems were single species with high cover and achieving multi-species LAI estimation in the low plant cover systems of arid rangelands has additional challenges (Smith et al. 2019). Estimating LAI of all present vegetation has been demonstrated over tree species in tropical forests (Park et al. 2019), and in a mangrove forest (Tian et al. 2017). However, UAS-derived estimates with cost effective red, green, and blue (RGB) of LAI of all present vegetation has remained untested in rangelands.

Estimating LAI in rangelands with UAS presents many challenges. Firstly, multiple species exist over short distances and a species-specific LAI estimation model, like those utilized in cropping systems, is impractical. Secondly, due to the heterogeneity in species and functional types from bare ground to bunchgrasses to shrubs and trees, there is also great variability in canopy height that produces shadows

in the imagery adjacent to and within vegetation. Shadows are a problem in high resolution UAS data because the low light conditions reduce feature extraction accuracy (Milas et al. 2017), and in many previous studies (e.g., Park et al. 2019; Buthelezi et al. 2023) shadows were masked or ignored. Finally, co-registration errors may offset the true location of the field-based observations and the truly co-located UAS pixels. These spatial uncertainties may propagate into modeled estimates of LAI.

Despite the potential challenges of using UAS to estimate LAI in rangelands, it is particularly enticing because UAS can rapidly cover areas as large as 1 ha at very high resolutions (< 1 cm^2). To date no current methods with UAS have been tested to estimate LAI in rangelands using cost effective RGB. Thus, the goal of this research is to model LAI of all vegetation at a very high resolution (< 1 cm^2) over a 1 ha Wyoming big sagebrush community by pairing a UAS acquisition with a limited and representative point intercept field sample. Given the heterogeneity of the vegetative cover and the spatial uncertainties between field data and UAS data, our objectives are to: (1) train a Random Forest (RF) model to estimate LAI using UAS spectral and structural data and (2) validate the trained RF model at the plot (1 m^2) scale, test the accuracy at the macroplot (1 ha) scale, and assess the within plot accuracy and impacts of shadows.

Methods

Study area

This study was conducted in the Reynolds Creek Experimental Watershed, a Long-Term Agroecosystem Research (LTAR) site near Murphy, Idaho, USA (Fig. 1). The 1 ha macroplot (43°10′13″ N, 116°43′20″ W) had an elevation of 1446 m and was dominated by Wyoming big sagebrush (*Artemisia tridentata* subsp. *wyomingensis*), bluebunch wheatgrass (*Pseudoroegneria spicata*), and Sandberg bluegrass (*Poa secunda*). Additionally, less common forbs and herbaceous vegetation were present in the study site that also contributed to the LAI. Invasive grasses such as cheatgrass (*Bromus tectorum*) are sparsely present in the study site; however, in the sampling locations cheatgrass was not measured. The mean annual precipitation was 271 mm and mean annual temperature was 8.8 °C (WRCC, 2024). Soils were well drained gravelly loam from the Mackey-Cottle associations denoted with typical profiles of A and B horizons with lithic bedrock (Soil Survey Staff, 2024). The site was representative of Wyoming big sagebrush communities in the Great Basin.

Field sampling

LAI measurements were recorded on June 3, 2021 near peak biomass for the site at 30 plots (1 m^2) that were randomly distributed and oriented at a randomly assigned azimuth within a 1 ha macroplot (Fig. 1). Azimuth values ranged from 0 to 360 degrees at intervals of 45 degrees. The corners of each plot were marked with a monument and measured with a Topcon Hiper V (Topcon Positioning Systems, Livermore, CA, USA) Real Time Kinematic (RTK) survey-grade global position system (GPS) with sub-centimeter accuracy. The corner monuments were vertically oriented PVC tubes that each plot leg could slide into for sampling. The sampled area, which is fully within the plot corners, represented a one square meter area and was designed in a quadrat scheme with 5 rows (20 cm apart) and 20 pin drop locations along each row (5 cm apart). The point intercept measurement device is a rigid system standing on four legs that slide into the monument locations. The measurement grid was elevated above the vegetation canopy and leveled with four bubble levels, one on each corner. A rigid rail with 20 notches to guide pin point measurement locations was set up in five positions, where each position corresponded to the rows of the quadrat scheme. The rigid system created a precise and repeatable sampling grid. For each plot, there are a total of 100 pin point samples to measure LAI. A sharpened pin, with infinitesimally small area, was manually dropped at each pin point location. While the pin was lowered from above the canopy to the ground surface, each time the pin encountered green vegetation a "hit" was recorded along with the vegetation species the pin hit. In our case, plot level LAI (1 m^2) was calculated as the ratio of m^2 of leaf area per m^2 of ground area sampled, or the ratio of green hits of the 100 pinpoint attempts (Clark and Seyfried 2001). At the macroplot scale (1 ha) LAI is calculated as the average of the representative sampling design of all 30 plot measurements. The manual and human component of LAI measurement

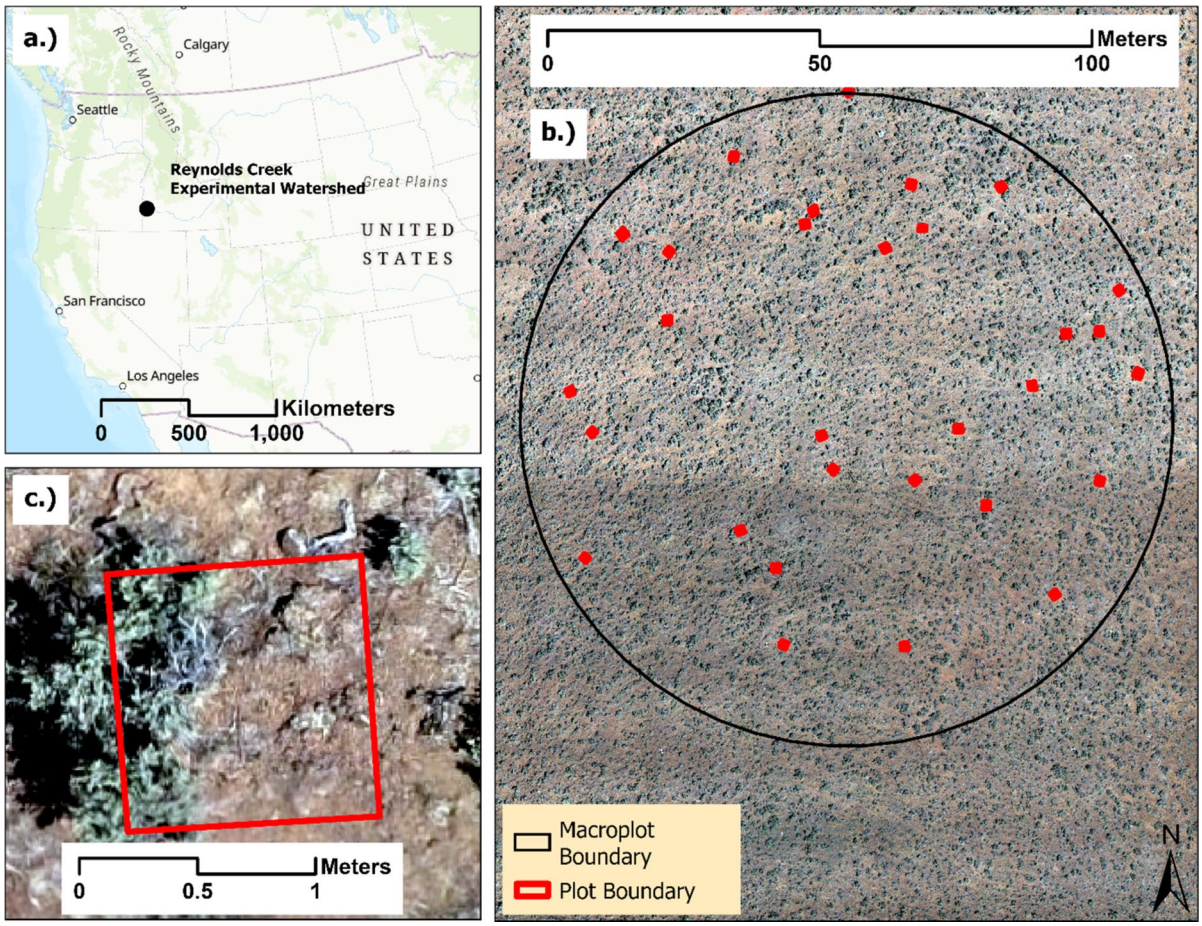

Fig. 1 The nested sampling design for estimating leaf area index (LAI) in the Reynolds Creek Experimental Watershed in southwestern Idaho, USA (**a**), with reference unoccupied aerial system (UAS) imagery (**b** and **c**) of the 1 ha macroplot, outlined in black (b), and a close-up view of a single plot, outlined in red (**c**)

with point intercept methods in a quadrat design can lead to variable hit counts at each pin point location, but differences in observer generally average out at the plot level. After a quality assessment we determined two of the plots were measured offset from their monument locations by a full meter due to human error setting up the point intercept measuring device and we excluded them from our analysis leaving a total of 28 plots.

UAS data acquisition

We collected UAS data over the 1 ha macroplot on June 3, 2021 near peak biomass of the site, with a DJI Phantom 4 to collect RGB data at nadir and off-nadir (65 degrees) camera angles to capture structural information within the plant canopy following methods described by Cunliffe et al. (2016). To minimize shadows the flight took place near solar noon. Flight height was 20 m, and forward and side overlap were 75%. The low flight height produced an average ground sample distance (GSD) of 8.31 mm/pixel. Thirteen black and white ground control points in a star pattern were measured with the RTK system to geo-reference the imagery. The RGB orthomosaic, dense point cloud, digital terrain model (DTM), and digital surface model (DSM) were calculated with structure from motion (SfM) photogrammetry software Agisoft Photoscan version 1.8.1. We report the accuracy (average error) and precision (standard deviation) of the SfM photogrammetry processing (James et al. 2019). The average x, y, and z error

(cm) when compared to the 13 ground control points was 3.86, 4.07, and 3.04, respectively. The standard deviation of the x, y, and z error (cm) was 2.96, 2.95, and 1.98, respectively. The resulting orthomosaic had a spatial resolution of 8.31 mm/pixel while the DTM and DSM had spatial resolutions of 16.6 mm/pixel.

Spatial interpolation

We used point intercept observations (quadrat design) in our study as ground truth measurements of LAI which covered a 1 m^2 plot, denoted as Point Intercept Sampling in Fig. 2. It is important to note the pin point observations theoretically have no area value and the UAS pixels have a spatial resolution of 8.31 mm/pixel. The difference in area between the pin point observations and the UAS pixel was a significant concern. Comparing a single pin point to a single pixel was problematic because LAI is a unitless value defined as the green leaf unit area per unit area. Point intercept sampling achieved an area value of 1 m^2 by calculating the ratio of green hits recorded at each of the 100 pins within the plot, where the pins are a representative sample. Our UAS pixels had an observed area (0.69 cm^2). Therefore, we could not directly assign the pin point measured hit value directly to the co-located UAS pixel.

As shown in our workflow diagram (Fig. 2), point intercept plots (n = 28) were initially split into training (n = 4) and validation (n = 24) sets. For all of the training plots we first generated the pin point measurement locations within each plot. Each plot consists of 100 pin points, distributed over 5 rows that were 20 cm apart, 20 points per row at 5 cm apart. Given these geometric guidelines, we generated the pin points with a geographic information system (GIS) workflow. The row orientation was determined by the plot azimuth. We acknowledge these generated points contain a certain level of spatial uncertainty from the GPS coordinates, human variability in measurement which may be significant, and locational error associated with generating the points that was difficult to quantify, potentially adding to the issues of co-registration.

The spatial resolution and unit differences between the pin point observations and the UAS data coupled

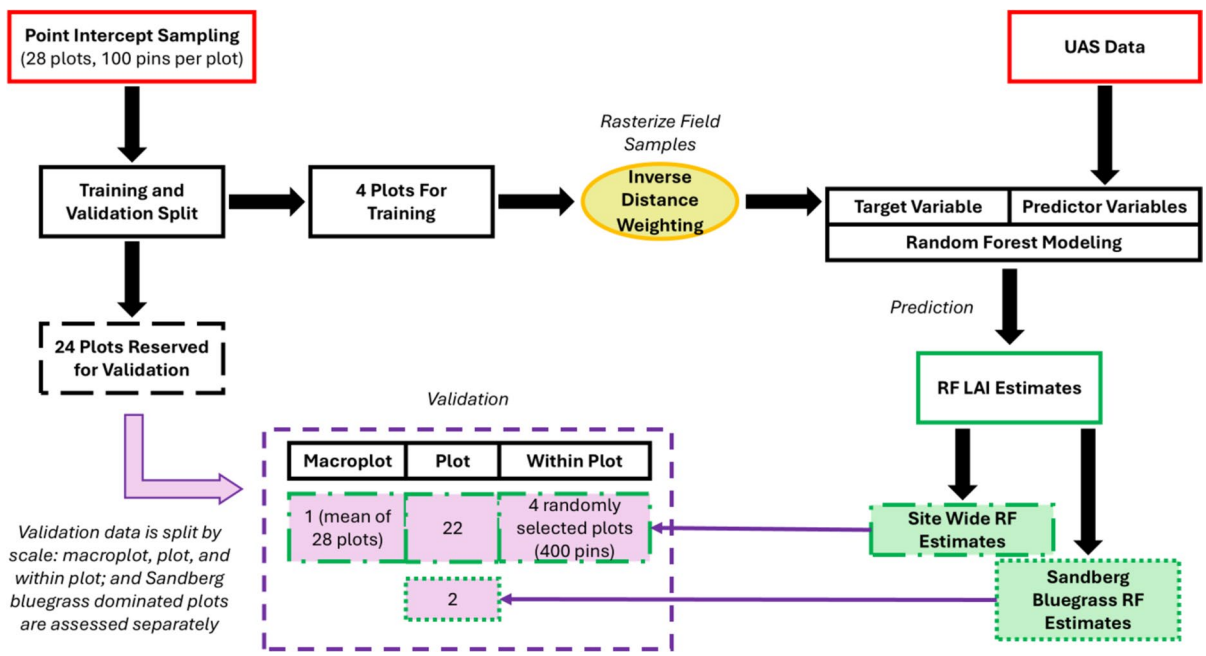

Fig. 2 Workflow diagram of the order of modeling operations with color coded steps from field observation of Point Intercept Samples and UAS acquisition to model validation at multiple scales. Data acquisition (red) is split into training and validation sets. Training data is rasterized with Inverse Distance Weighting (yellow) and paired with UAS data (red) to train two Random Forest models (green). Modeled estimates are validated with the point intercept sampling data (purple) at the macroplot, plot, and within plot scales

with co-registration errors in the GPS and UAS data motivated us to spatially interpolate the point intercept field observations. For the four training plots, we used Inverse Distance Weighting (IDW) as a preprocessing step (Fig. 2, yellow oval) to rasterize the pin point observation to the resolution of the UAS raster grid. The resulting IDW interpolated training surface estimated the continuous LAI value at a given location as a weighted mean of the nearby pin point observation defined by Eq. 1, where the calculated weight w_i was multiplied by the observed LAI_i (Brunsdon and Comber 2015). The distance weight w_i was calculated by Eq. 2 where a positive α determined how the distance between two observations (x and x_i) was treated. IDW was performed with the "gstat" package in R version 4.4.0 (Pebesma EJ 2004; Gräler et al. 2016; R Core Team 2024). The four training plots were representative of four dominant vegetation types in the study macroplot: Wyoming big sagebrush, bluebunch wheatgrass, Sandberg bluegrass, and barren. Dominant means the contribution of LAI was dominantly from a single vegetation species even though other species existed within the plot.

$$LAI_{IDW}(x) = \frac{\sum_i w_i LAI_i}{\sum_i w_i} \quad (1)$$

Development of an IDW interpolated training surface for four training plots accomplished two important steps: first, the area discrepancy between pin point LAI hit observation and pixel was resolved by producing continuous float LAI interpolated values for every pixel, and second, the location of the observed LAI was smoothed reducing the importance of offset issues associated with field sample to UAS data co-registration. Due to the sensitivity of IDW to edge effects the interpolation area only covered 0.76 m^2 of each of the four training plots or the outermost extent of the sampled area. Ten values of α (1 through 10 at intervals of 1) were tested and compared visually with the UAS reference imagery. Selection of α was done based on the visual representativeness of the resulting IDW interpolated training surface. Accurate representation of the space between the generated pin point locations was paramount, which is why a visual assessment was most appropriate.

$$w_i = |x - x_i|^{-\alpha} \quad (2)$$

Random forest modeling

Random forests (RF) are a tree based supervised machine learning method appropriate for classification and regression modeling (Breiman 2001). RF's are broadly applied in remote sensing, and were selected in this research to model LAI because RF's are generally robust to overfitting even with highly correlated variables such as the UAS variables we derive, discussed below (Belgiu and Drăguţ 2016). We used the 'randomForest' package in R (Wiener 2002).

Predictor selection was iterative. Two sources of raw data were used in the model: RGB spectral indices and the canopy height model derived from the digital surface model (DSM) minus the digital terrain model (DTM). The canopy height model was resampled to

Table 1 Color and texture features used to estimate LAI in the final RF model

Feature Name	Abbreviation	Equation	Reference
RGB Chromatic Coordinates	R_{CC}	$R_{CC} = R/(G+R+B)$	Park et al. (2019)
	G_{CC}	$G_{CC} = G/(G+R+B)$	
	B_{CC}	$B_{CC} = B/(G+R+B)$	
Excess Greenness	ExG	ExG = 2*G—(R + B)	Park et al. (2019)
Canopy Height	CHM	CHM = DSM—DTM	–
Low Pass Filter	LP_R	3 × 3 moving window average	Jensen (2016)
	LP_G		
	LP_B		
High Pass Filter	HP_R	3 × 3 moving window weighted average	Jensen (2016)
	HP_G		
	HP_B		

R red, *G* green, *B* blue, *DSM* digital surface model, *DTM* digital terrain model

the RGB resolution with a bi-cubic interpolation. As shown in Table 1, we selected the RGB chromatic coordinates, excess greenness, canopy height, and two filters with a 3 by 3 moving window. The filters were applied because we do not discard the shadowed pixels and contextual neighborhood values may be important for estimating LAI in a shadowed pixel. Predictor data extent matched the IDW interpolated training surface extent.

The RF model was trained to estimate the target variable, the four IDW interpolated training surfaces (Fig. 2), using the predictor variables listed in Table 1. Predictor variables were clipped to the extent of the IDW interpolated training surfaces. We tested many other predictors including standard deviation of red, green, and blue; however, using the variable importance plot we discarded non-important predictors to reduce computation times and potentially increase model performance. The purpose of the workflow was to assess whether a RF model could be trained to estimate LAI at a high resolution over a 1 ha macroplot by pairing UAS data with a limited and representative point intercept field sample. As shown in Fig. 2, two RF models were developed: one site wide RF model (trained with 3 IDW interpolated training surfaces as the target variable and the associated predictor variables) and one RF model specific to Sandberg bluegrass (trained with 1 IDW interpolated training surface as the target variable and the associated predictor variables).

Validation

Validating the RF estimated LAI was completed at the 1 m^2 plot scale and within plot scale and tested at the macroplot scale (1 ha). As shown in Fig. 2, the plot scale validation data was split into two categories: site wide testing at the scale macroplot (n = 1) scale, and validation at the plot (n = 22), and within plot (n = 4, randomly sampled plots) scales. We validated the Sandberg bluegrass RF model estimated LAI at the plot level (n = 2) because only 3 plots in total were dominated by Sandberg bluegrass. We tested the site wide RF model estimate accuracy at the macroplot scale. We tested macroplot accuracy two ways: by averaging the estimated LAI for pixels within the 28 plots and averaging the estimated LAI for all pixels within the macroplot. Macroplot measured LAI was calculated as the average of plot measured LAI (n = 28). As shown in Fig. 2, macroplot testing was assessed with the site wide RF model. Sandberg bluegrass existed throughout the macroplot, but in order to estimate LAI of Sandberg bluegrass separately one would need to accurately map and classify vegetation at the species level. Currently, species level mapping has not been demonstrated in complex rangelands at the resolution of UAS data used in this study.

Plot level validation of the site wide RF model and the Sandberg bluegrass RF model required additional consideration. Point intercept plot measured LAI is representative of and calculated for an area of 1 m^2. The plot monument corners extend well beyond 1 m^2 due to the design of the point intercept sampling system, and to resolve the area mismatch we generated an exactly 1 m^2 validation square. The Sandberg bluegrass specific model was developed to assess whether RF could be implemented to resolve species specific issues at the plot level. Plot level RF modeled LAI estimates were calculated as the sum of the LAI pixel values divided by the pixel count within the 1 m^2 validation boundary. At the plot level we calculated the Mean Absolute Error, Root Mean Squared Error, and R-squared of the combined results of the site wide RF model plus the Sandberg bluegrass model (see validation data splits Fig. 2).

Additionally, we validated the site wide RF model within plot mean accuracy for shadow and shadow free pixels. An important component of our workflow is the inclusion of shadow covered pixels in the training and validation of the RF model estimates of LAI. We directly compared individual pin point measurements within four randomly selected plots to the site wide RF model LAI estimates (Fig. 2, validation). Because of the importance of co-registration of very high resolution UAS data to field data with GPS errors and human error in sampling we also assessed the site wide RF model LAI estimate within a 5-cm diameter buffered area about each pin point measurement location to the pin point measured LAI. For both the direct pin point to pixel and the pin point to buffered comparison we visually assigned a shadow value as either shadow impacted pixels (directly within full shadow or directly adjacent to a full shadow) or shadow free pixels. The buffering step and the visual shadow assignment which included adjacent pixels was conducted to offset the potential co-registration errors and the pin to pixel comparison issue that

motivated us to implement IDW as discussed earlier in the methods. For both the pin point to pixel and the pin point to buffered comparison we compared the mean full site RF model LAI with the mean pin point measured LAI. Due to the area discrepancy between pin points and pixels we analyzed the within plot mean totals to determine whether shadows posed a significant reduction in overall plot accuracy.

Results

Spatial interpolation

Inverse distance weighting was applied to address the area mismatch between UAS and field observations and smooth the location of the generated points within the four training plots (Fig. 2) over the UAS grid. The resulting IDW interpolated training surface contained continuous LAI values for each pixel at a spatial resolution of 8.31 mm/pixel. Figure 3 shows the generated points and IDW interpolated training surfaces for two selections of α (1 and 5), which determines the weighting of an observation for a given distance, for training plot number 30. The IDW

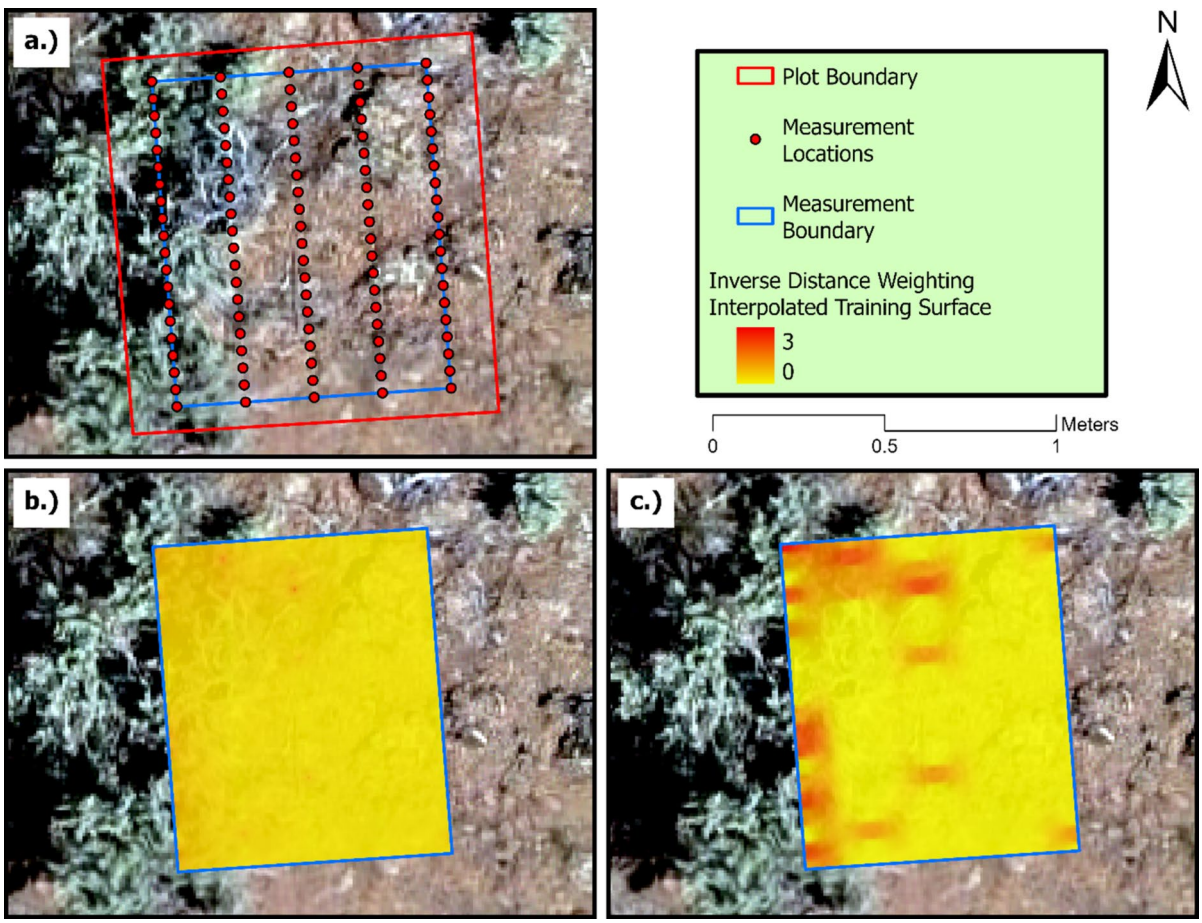

Fig. 3 Leaf area index (LAI) interpolated from 100 points (**a**) to the measurement boundary (blue rectangle) within the 1 m^2 plot (red outline) using *inverse distance weighting* (IDW) *with* two distance weights (α). A lower weight (α = 1) leads to a smoothed average surface that underrepresents the minimum and maximum (**b**), while a higher value (α = 5) had more zero values (**c**) and was a better match to the unoccupied aerial system (UAS) imagery

interpolated training surface is visibly different for the two different values of α. When α is small (Fig. 3b) the range in interpolated values was also small (LAI = 0–1.6). When α was increased to five (Fig. 3c) the range in LAI increased to 3 (0–3), which matches the observed range in pin point measured LAI. The IDW interpolated training surface for an α of five was more realistic, matching the green vegetation visible in the reference imagery (Fig. 3a). Areas where we expect zero LAI are reasonably represented with an α of five. In contrast, with an α of one, areas where we expect a LAI of zero are overestimated compared to the reference imagery. We determined an α of 5 to be appropriate because increasing α to 6 or more did not add any value to the spatial representativeness of the IDW interpolated training surfaces. IDW smoothing accomplished a few important adjustments to the pin point (quadrat design) observations in a plot: IDW successfully represented the space between generated pin point locations, converted the count data to a more realistic continuous value for each pixel (resolving unit discrepancies), increased the amount of training data 100-fold (100 points versus over 10,000 pixels), and interpolated LAI in shadow obscured pixels. We acknowledge the increase in training data achieved through IDW may degrade the accuracy of the actual field observations; however, manual collection of 10,000 observations is impractical and the workflow presented pairs UAS acquisition with a limited and representative point intercept sample (n = 4 plots) to model LAI for an entire hectare greatly increasing data collection time savings. We produced an IDW interpolated training surface for four representative plots as a preprocessing step of the field sample point intercept (quadrat design) data (Fig. 2).

Random forest modeling

Two RF models were developed (Fig. 2). One site wide RF model was trained using IDW interpolated training surfaces from three plots representative of Wyoming big sagebrush, bluebunch wheatgrass, and barren plots. One Sandberg bluegrass RF model was trained using an IDW interpolated training surface for a single plot representative of Sandberg bluegrass. All pixels within the measurement boundary (0.76 m^2) for the IDW interpolated training surface (target variable) and UAS features (predictors) were used to train the RF models. The site wide RF model performed well for all vegetation types aside from plots whose LAI was dominated by Sandberg bluegrass. Variable importance in the site wide RF model was in the following order: CHM, b_{cc}, r_{cc}, g_{cc}, LP_R, LP_B, LP_G, HP_B, HP_G, HP_R, and finally ExG. The site wide RF model had a mean squared error (MSE) of 0.28; however, it is important to note the MSE was derived based on the IDW interpolated training surface and as shown in Fig. 2, validation is only conducted on the field sampled data. The resulting MSE is therefore a reflection of the site wide RF model performance as measured against the preprocessing step of IDW interpolation and is not indicative of model performance against the field sampled data.

A visual assessment of the site wide RF model estimated LAI for two randomly selected plots from the validation set is shown in Fig. 4. The complexity of LAI represented by the site wide RF model LAI estimates surpassed the spatial complexity visually apparent in the IDW interpolated training surface (Fig. 3c). Wyoming big sagebrush has sage green colored leaves (Fig. 4a, c) and had the highest contribution of LAI in the plots shown, which correspond to the darker green pixels in the LAI estimation (Fig. 4b, d). LAI for herbaceous cover is also apparent by the darker green color (center of the plot boundary (Fig. 4d). Visually, the herbaceous cover appears brown in the reference imagery (Fig. 4a, c), which is discussed in detail below. Bare ground is visually represented well in Fig. 4.

Validation

Initially we trained a RF model with all four IDW interpolated training surfaces (Fig. 2), which would have resulted in a single RF model; however, RF model performance was relatively poor when compared with all 24 validation plots ($r^2 = 0.39$). Upon further inspection, the RF model trained with four IDW interpolated training surfaces underestimated LAI in the only three plots dominated by Sandberg bluegrass, two plots from the validation set and one plot from the training set. To resolve the Sandberg bluegrass issue we developed two RF models, one full site RF model trained with three IDW interpolated training surfaces representative of Wyoming big sagebrush, bluebunch wheatgrass, and barren, and one Sandberg bluegrass RF model trained with a single

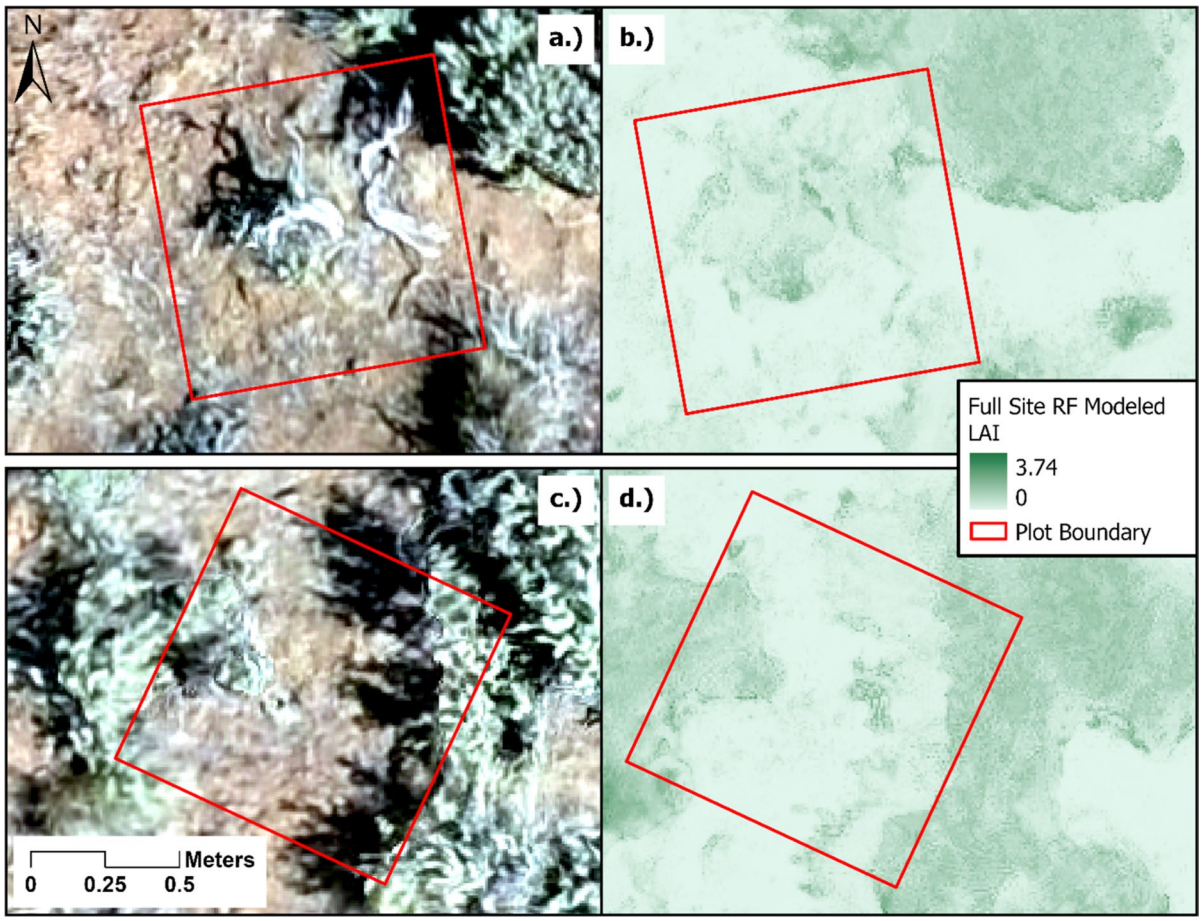

Fig. 4 The unoccupied aerial system (UAS) true color orthomosaic for plot 3 (**a**) and plot 19 (**c**) and the resulting Random Forest (RF) model estimated leaf area index (LAI) predictions are shown for plot 3 (**b**) and plot 19 (**d**). High LAI is depicted in dark green and low LAI is light green. The reference image in the left column shows the variability of vegetation and the presence of shadows and the right column shows the variability in the predicted LAI within the plot

IDW interpolated training surface representative of Sandberg bluegrass. The site wide RF model performed well at the plot level with an $r^2 = 0.72$, compared with the 22 plots from the validation set that were not dominated by Sandberg bluegrass (Fig. 2, validation). Because Sandberg bluegrass is prevalent in the study site, we combined the results of the site wide RF model (n = 22, plots) with the Sandberg bluegrass RF model (n = 2, plots) to assess plot level accuracy. At the plot level, measured LAI was the ratio of the hits, and modeled LAI was the average of the estimated LAI pixels within the 1 m^2 validation plot boundary. The measured plot LAI and estimated LAI are collectively plotted in Fig. 5 ($r^2 = 0.69$, MAE = 0.08, RMSE = 0.10). The Sandberg bluegrass specific RF model appears to more closely follow the dotted one-to-one line (Fig. 5, solid black points), although we cannot draw any conclusions because there are only two points. The full site RF model generally overestimates lower values of LAI and underestimates larger values (Fig. 5), even though the relationship is linear between RF modeled and plot measured LAI.

We also compared the site wide RF model estimated LAI with the measured LAI at the macroplot scale. Because Sandberg bluegrass is prevalent and it is impractical to model Sandberg bluegrass separately at the macroplot scale, we compared the site wide RF model LAI estimates

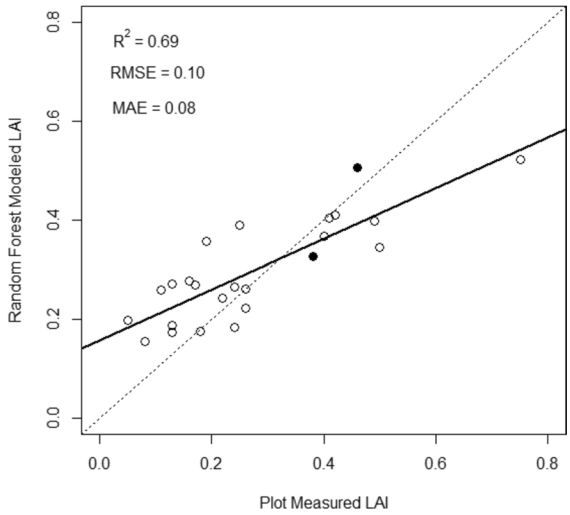

Fig. 5 Random Forest (RF) predicted leaf area index (LAI) for each validation plot (n = 24) is plotted against the measured leaf area index. The Sandberg bluegrass RF model results are plotted as solid black points. The model fit is shown as a solid line, and the 1:1 line (dotted) is shown for reference

(average value over the macroplot) with the average value of the measured LAI (28 randomly distributed plots, that are representative of the macroplot). It is important to note the field measured LAI is a representative sample covering only 28 square meters, or 0.28% of the 1 ha macroplot. We first calculate the direct comparison, or the average of the RF model estimated LAI within the plots (28 m^2) to mimic the field sample design. We found the RF model estimated LAI is 0.28, which is equal to the field measured LAI of 0.28. By considering all of the pixels within the macroplot we found a slightly higher RF model estimated LAI of 0.345.

We quantified the shadow impacts on within plot RF model LAI estimate accuracy of four randomly selected plots from the validation set (Fig. 2, validation). We generated pin point measurement locations for the four randomly selected plots. For each pin point within the four randomly selected plots, we visually recorded whether the co-located pixel was shadow affected or not in the RGB imagery. This representative sample included 400 pin point locations that were used to assess within plot shadow impacts. A direct comparison of the site wide RF model LAI estimates to the measured LAI at each pin point would be incorrect because of the area difference between the pin point (no area value) and the pixel (area of 0.69 cm^2). Therefore, we compared the mean site wide RF model LAI estimates with the pin point measured LAI for shadow affected pixels (Table 2). We compared the mean no shadow pin point measured LAI with the mean of the co-located site wide RF model LAI estimate. For each pin point we also created a 5 cm diameter buffered area and calculated the mean site wide RF model LAI within the buffer to mitigate potential co-registration

Table 2 The impact of shadows in the unoccupied aerial system (UAS) imagery on the Random Forest (RF) model estimated leaf area index (LAI) is shown for four randomly selected plots from the validation set (400 points in total)

Plot Number	Shadow Denotation	Measured LAI	Modeled LAI Point to Pixel	Modeled LAI Buffered 5 cm	Count
3	No Shadow	0.117	0.229	0.239	77
	Shadow Affected	0.087	0.418	0.389	23
7	No Shadow	0.296	0.346	0.357	81
	Shadow Affected	0.842	0.375	0.385	19
8	No Shadow	0.241	0.235	0.235	87
	Shadow Affected	0.077	0.243	0.193	13
17	No Shadow	0.521	0.361	0.367	96
	Shadow Affected	0.000	0.632	0.570	4
Totals	No Shadow	0.305	0.295	0.302	341
	Shadow Affected	0.322	0.380	0.357	59
	Cumulative LAI	0.308	0.308	0.310	400

The mean point measured LAI, the single pixel mean modeled LAI co-located with the point, the 5-cm diameter buffered modeled mean LAI about the co-located point, and the count of data points are presented in the columns. Each point was assigned a value of shadow free or shadow affected. The mean LAI values are also summarized

errors. The site wide mean RF estimated LAI for the co-located pixel (0.308) and for the buffered area (0.310) is nearly equivalent when compared to the measured (0.308) LAI (given as bold totals in Table 2). A total of 59 out of 400 (14.75%) pin point measurement locations were co-located with a shadow affected pixel. Within plot mean site wide RF model LAI shadow affected estimates were also very similar to the measured LAI (point to pixel: 0.380, point to buffer 0.357, and measured 0.322). Within individual plots we noted more variability between measured LAI and RF modeled LAI. Co-located pixels that were shadow free had more similar mean measured LAI compared to the modeled LAI than the shadow affected pixels; however, the total difference in mean LAI was small as seen in the totals (Table 2). The difference or residual between measured and point to pixel modeled LAI in shadow affected pixels was 0.06 calculated as the difference between the bolded measured shadow (0.322) and modeled point to pixel (0.380) totals (Table 2).

Discussion

We demonstrate in this study that LAI of all present vegetation species can be modeled with point intercept plots, visual RGB UAS data, and RF machine learning models. Very high resolution (<1 cm^2) RGB-based indices and a canopy height model derived from structure from motion were the only predictors needed to achieve accurate results. We accomplished this by transforming the plot data using inverse distance weighting which increased the training data of LAI from 100 points per plot to over 10,000 pixels per plot. This important step address two basic difficulties when comparing the measured LAI and UAS data: differences in area between pin point observations (no area) and pixels (0.69 cm^2), and co-registration errors (smoothed by IDW). Addressing these difficulties allowed us to develop a site wide RF model to estimate LAI of the present vegetation species and we obtained r^2 values of 0.72 excluding Sandberg bluegrass and 0.69 for the combined output of the full site and Sandberg bluegrass RF models, which is similar to other published work using a Random Forest and RGB UAS data to estimate LAI of maize (r^2 of 0.71–0.88 (Du et al. 2022)). We presented a paired approach where UAS data is collected alongside a representative limited field sample ($n=3$ plots for the site wide RF model) of point intercept LAI (quadrat design) to train and model LAI over a 1 ha macroplot at an 8.31 mm/pixel spatial resolution. In rangelands there is additional complexity because of the multitude of vegetation species present that all green up at different times, and further validation of the method detailed here across a full growing season is warranted.

The site wide RF model in our study performed well at plot level. At the macroplot level (1 ha) we found similar results for within plot average LAI and slightly higher RF model estimated LAI when all pixels within the macroplot were considered. Our macroplot comparison shows the promise of using UAS for LAI estimation, which has more complete coverage than the randomly distributed field plots; however, these methods should be tested across a range of sites with additional macroplots for validation. We also analyzed the within plot impacts of shadows, which differed from other research where shadows were either not discussed or discarded completely (e.g., Park et al. 2019; Buthelezi et al. 2023). One difficulty of shadows is that low light conditions may reduce feature extraction accuracy, and Milas et al. (2017) demonstrated modeling shadows separately can increase the overall accuracy of feature mapping. In our study the average LAI estimates in shadowed areas were better than the individual within plot estimates, which had some variability. The difficulty the site wide RF model had representing the variability of shadow affected pixels for individual plots is unsurprising because shadows within a canopy may have far different LAI than shadows outside of a canopy. On average the site wide RF model LAI estimates for shadow affected pixels was very similar to the measured LAI (0.380 versus 0.322, respectively). Minimizing shadows during UAS acquisition by flying near solar noon is important due to the widespread existence of shadows and their strong contrast between soils, background, and biocrusts in rangelands (Roser et al. 2022). Discarding shadows completely may not be a reasonable option in rangelands because excluding shadow affected pixels could misrepresent the obscured portion of LAI. Although the within plot mean site wide RF model LAI accuracy for shadow affected pixels was similar to the measured

LAI, future research should attempt modeling LAI of shadow affected pixels separately from shadow free pixels.

The variability of LAI in rangelands is visually apparent in the UAS reference imagery used in this study, which is lost in the spatial generalization of satellite based remote sensing products. Even comparing MODIS satellite-based remote sensing LAI products, estimates vary a great deal (e.g., MCD15 and Global Land Surface Satellite (GLASS)) and introduces uncertainty into carbon and water cycle modeling (Liu et al. 2018). Evapotranspiration (ET) and Gross Primary Production (GPP) are both important outputs from carbon and water models and it has been demonstrated that these are sensitive (errors as large as 20%) to LAI (Heinsch et al. 2006; Ryu et al. 2011). The benefit of the satellite-based remote sensing products is their temporal and spatial coverage, which address the significant under sampling issue associated with field-based techniques. UAS has the potential to fill the gap between field and satellite-based scales, with high accuracies, and relatively large spatial and temporal coverage, that can be achieved by re-flying a site. While re-flying a site may introduce differences in viewing angle and solar illumination, the method detailed here uses a limited field sample (n = 3–4, 1 m^2 plots) paired with a UAS acquisition to train a RF model to estimate LAI of an entire hectare and the paired approach may mitigate the different conditions for each UAS acquisition. Scaling the carbon and water cycle for a site down to the plot (1 m^2) and the pixel (1 cm^2) is currently difficult with remote sensing, but a comprehensive physical model of carbon and water cycling could be greatly aided by the very high resolution, accurate, and spatially heterogeneous LAI estimates achievable by UAS.

Limitations

Although our full RF model of LAI performed well over nearly all the vegetation types, the model underestimated Sandberg bluegrass, a small stature grass, even when we incorporated Sandberg bluegrass in the training data. Ultimately, we developed a Sandberg bluegrass specific model that produced equivalent results to the full model over plots dominated by this vegetation. The non-photosynthetic vegetation for Sandberg bluegrass may be visually substantial. Interestingly, in our site wide RF model the LAI of Sandberg bluegrass was underestimated highlighting difficulty of LAI estimation of small stature grasses with large amounts of non-photosynthetic vegetation. Sandberg bluegrass has fine vertically oriented leaves and LAI is easy to underestimate with remote sensing at the nadir view. Additionally, in this Wyoming big sagebrush community early June is likely past peak greenness for Sandberg bluegrass, which keeps its leaves tightly rolled to avoid transpiration losses due to drought stress (Link et al. 1990). The dead and senescing materials of Sandberg bluegrass also lay flat which may lead to overestimation of dead material from nadir remote sensing (e.g., Mayr and Samimi 2015). The density of grass coverage is also important and a combination of low density and low greenness may lead to underestimation (Sha et al. 2019). Estimating LAI of small-stature grasses with large amounts of non-photosynthetic vegetation like Sandberg bluegrass may be more successful if LAI estimation models were developed for each plant functional type, or image collection spanned a temporal window (Wood et al. 2022).

Our study used point intercept plots as the LAI reference, which describe 96% of the variability in LAI for all the vegetative species present in Wyoming big sagebrush communities (Clark and Seyfried 2001). If we had used destructive sampling the measured LAI may have differed; however, the study site was established for long term vegetation monitoring and destructive sampling was not a viable option. Comparing the plots to UAS data introduces a spatial issue: identifying the exact measurement location of each observation within the plot. Each plot corner was surveyed with a highly accurate RTK system; however, the point intercept measurement locations, or pins, within the plot had to be estimated. We expect some location uncertainty between the generated measurement locations within each plot and the actual measurement location. We attempted to mitigate these spatial uncertainties, which are present in all UAS to observation comparisons, by applying IDW to interpolate observation locations. This step may help address the spatial uncertainty, but also may introduce incorrect LAI representation between pins. Additionally, the spatial uncertainty in the processed UAS imagery was larger than our pixel size (8.31 mm) which may impact the training relationships between field samples and UAS pixels. With advances in technology UAS data locational

accuracy may be increased potentially reducing the need to apply inverse distance weighting as presented in this work, which helps to overcome the spatial uncertainty.

Conclusions

This study provides an important step towards broad application of UAS to retrieve LAI by demonstrating a trained RF model can accurately estimate LAI at multiple scales over a diverse range of species characteristic of Wyoming big sagebrush communities ($r^2 = 0.69$ compared to reference point intercept plots). Our workflow pairs a UAS acquisition with a representative and limited ($n = 3$ plots for our site wide RF model) field sample to accurately estimate LAI over a 1 ha macroplot. Future research should investigate the transferability of this methodology to different sites across an elevational gradient of plant communities common to rangelands in the Great Basin. The timing of image acquisition may impact the model if the paired UAS plus field data collection cannot be completed on the same day, and an assessment of multiple images throughout the growing season would further validate this approach. A plant functional type-based model of LAI may address the species-specific issue we noted when estimating LAI over Sandberg bluegrass, which is a logical next step because UAS protocols for mapping plant functional type with high accuracy in rangelands are well established (e.g., Roser et al. 2022). Rapid and accurate quantification of leaf area index of all present vegetation in vast rangelands is faced with two problems: first, accurate field based results require significant time to collect thereby limiting their coverage, and second, satellite-based remote sensing products are often too coarse in spatial resolution to represent the subtle vegetation dynamics, especially in rangelands dominated by woody shrubs like Wyoming big sagebrush (Fremgen-Tarantino et al. 2021; Applestein and Germino 2022). UAS offers an enticing middle ground because accurate and cost effective RGB data can be quickly collected at a fine spatial resolution (< 1 cm^2) over areas of meaningful size with a limited number of point intercept plots (quadrat design) to quickly estimate LAI one hectare at a time. LAI is an important variable for carbon and water modeling that rapidly changes with environmental conditions, season, and species; and this study demonstrates UAS can be an accurate tool for estimating LAI adding to the ever growing toolbox of UAS-derived rangeland metrics (Gillan et al. 2020).

Acknowledgements This research was supported by the United States Department of Agriculture Agricultural Research Service, Northwest Watershed Research Center in Boise, Idaho in collaboration with the landowners within the Reynolds Creek Experimental Watershed and Critical Zone Observatory. This research was a contribution from the Long-Term Agroecosystem Research (LTAR) network. LTAR is supported by the United States Department of Agriculture.

Author contributions Study design and conception was performed by Craig Woodruff and Pat Clark. Data collection and UAS processing was conducted by Peter Olsoy. Material preparation and analysis was conducted by Craig Woodruff. The first draft of the manuscript was written by Craig Woodruff and all authors commented on previous drafts.

Funding This project was funded by the United States Department of Agriculture Agricultural Research Service (USDA-ARS).

Data availability The data used in this study will be available for researchers in the US Department of Agriculture's Ag Data Commons repository upon acceptance.

Declarations

Competing interests The authors declare no competing interests.

References

Applestein C, Germino MJ (2022) How do accuracy and model agreement vary with versioning, scale, and landscape heterogeneity for satellite-derived vegetation maps in sagebrush steppe? Ecol Ind 139:108935.

Beerling DJ, Fry JC (1990) A comparison of the accuracy, variability and speed of five different methods for estimating leaf area. Ann Bot 65:483–488.

Belgiu M, Drăguţ L (2016) Random forest in remote sensing: a review of applications and future directions. ISPRS J Photogramm Remote Sens 114:24–31.

Bonan G (1993) Importance of leaf area index and forest type when estimating photosynthesis in boreal forests. Remote Sens Environ 43:303–314.

Bonan GB (2016) Ecological climatology: concepts and applications, 3rd edn. Cambridge University Press, New York

Bonham CD (2013) Measurements for terrestrial vegetation, Second edition. Wiley-Blackwell, Chichester, West Sussex, UK ; Hoboken, NJ

Breiman L (2001) Random FORESTS. Mach Learn 45:5–32.

Brunsdon C, Comber L (2015) An introduction to R for spatial analysis and mapping. SAGE, Los Angeles London New Delhi Singapore Washington DC

Buthelezi S, Mutanga O, Sibanda M et al (2023) Assessing the prospects of remote sensing maize leaf area index using UAV-derived multi-spectral data in smallholder farms across the growing season. Remote Sens 15:1597.

Chen JM (1996) Evaluation of vegetation indices and a modified simple ratio for boreal applications. Can J Remote Sens 22:229–242.

Chen Z, Wang W, Cescatti A, Forzieri G (2023) Climate-driven vegetation greening further reduces water availability in drylands. Glob Change Biol 29:1628–1647.

Clark PE, Seyfried MS (2001) Point sampling for leaf area index in sagebrush steppe communities. J Range Manag 54:589.

Comba L, Biglia A, Ricauda Aimonino D et al (2020) Leaf area index evaluation in vineyards using 3D point clouds from UAV imagery. Precision Agric 21:881–896.

Córcoles JI, Ortega JF, Hernández D, Moreno MA (2013) Estimation of leaf area index in onion (Allium cepa L.) using an unmanned aerial vehicle. Biosys Eng 115:31–42.

Cunliffe AM, Brazier RE, Anderson K (2016) Ultra-fine grain landscape-scale quantification of dryland vegetation structure with drone-acquired structure-from-motion photogrammetry. Remote Sens Environ 183:129–143.

Delegido J, Verrelst J, Meza CM et al (2013) A red-edge spectral index for remote sensing estimation of green LAI over agroecosystems. Eur J Agron 46:42–52.

Du L, Yang H, Song X et al (2022) Estimating leaf area index of maize using UAV-based digital imagery and machine learning methods. Sci Rep 12:15937.

Enterkine J, Caughlin TT, Dashti H, Glenn NF (2024) Applied soft classes and fuzzy confusion in a patchwork semi-arid ecosystem: Stitching together classification techniques to preserve ecologically-meaningful information. Remote Sens Environ 300:113853.

Fan L, Gao Y, Brück H, Bernhofer Ch (2009) Investigating the relationship between NDVI and LAI in semi-arid grassland in Inner Mongolia using in-situ measurements. Theor Appl Climatol 95:151–156.

Finzel JA, Seyfried MS, Weltz MA et al (2012) Indirect measurement of leaf area index in sagebrush-steppe rangelands. Rangel Ecol Manage 65:208–212.

Fremgen-Tarantino MR, Olsoy PJ, Frye GG et al (2021) Assessing accuracy of GAP and LANDFIRE land cover datasets in winter habitats used by greater sage-grouse in Idaho and Wyoming, USA. J Environ Manage 280:111720.

Gillan JK, Karl JW, Van Leeuwen WJD (2020) Integrating drone imagery with existing rangeland monitoring programs. Environ Monit Assess 192:269.

Gong Y, Yang K, Lin Z et al (2021) Remote estimation of leaf area index (LAI) with unmanned aerial vehicle (UAV) imaging for different rice cultivars throughout the entire growing season. Plant Methods 17:88.

Hao L, Pan C, Fang D et al (2018) Quantifying the effects of overgrazing on mountainous watershed vegetation dynamics under a changing climate. Sci Total Environ 639:1408–1420.

Hasan U, Sawut M, Chen S (2019) Estimating the leaf area index of winter wheat based on unmanned aerial vehicle RGB-image parameters. Sustainability 11:6829.

Heinsch FA, Zhao M, Running SW et al (2006) Evaluation of remote sensing based terrestrial productivity from MODIS using regional tower eddy flux network observations. IEEE Trans Geosci Remote Sensing 44:1908–1925.

Hoek Van Dijke AJ, Mallick K, Schlerf M et al (2020) Examining the link between vegetation leaf area and land–atmosphere exchange of water, energy, and carbon fluxes using FLUXNET data. Biogeosciences 17:4443–4457.

Hunt ER Jr, Everitt JH, Ritchie JC et al (2003) Applications and research using remote sensing for rangeland management. Photogramm Eng Remote Sens 69:675–693.

James MR, Chandler JH, Eltner A et al (2019) Guidelines on the use of structure-from-motion photogrammetry in geomorphic research. Earth Surf Processes Landf 44:2081–2084.

Jensen JR (2016) Introductory digital image processing: a remote sensing perspective, 4th ed. Pearson Education, Glenview, Ill

Kalisperakis I, Stentoumis Ch, Grammatikopoulos L, Karantzalos K (2015) Leaf area index estimation in vineyards from uav hyperspectral data, 2D image mosaics and 3D canopy surface modelS. Int Arch Photogramm Remote Sens Spatial Inf Sci. https://doi.org/10.5194/isprsarchives-XL-1-W4-299-2015

Link SO, Gee GW, Downs JL (1990) The effect of water stress on phenological and ecophysiological characteristics of cheatgrass and sandberg's bluegrass. J Range Manag 43:506.

Liu Y, Xiao J, Ju W et al (2018) Satellite-derived LAI products exhibit large discrepancies and can lead to substantial uncertainty in simulated carbon and water fluxes. Remote Sens Environ 206:174–188.

Liu Z, Guo P, Liu H et al (2021) Gradient boosting estimation of the leaf area index of apple orchards in UAV remote sensing. Remote Sens 13:3263.

MacBean N, Scott RL, Biederman JA et al (2021) Dynamic global vegetation models underestimate net CO_2 flux mean and inter-annual variability in dryland ecosystems. Environ Res Lett 16:094023.

Mayr M, Samimi C (2015) Comparing the dry season in-situ leaf area index (LAI) derived from high-resolution RapidEye imagery with MODIS LAI in a namibian savanna. Remote Sens 7:4834–4857.

Mendes Dos Santos L, Ferraz GAES, Barbosa BDDS et al (2020) Determining the leaf area index and percentage of area covered by coffee crops using UAV RGB images. IEEE J Sel Top Appl Earth Obs Remote Sens 13:6401–6409.

Milas AS, Arend K, Mayer C et al (2017) Different colours of shadows: classification of UAV images. Int J Remote Sens 38:3084–3100.

Mougin E, Demarez V, Diawara M et al (2014) Estimation of LAI, fAPAR and fCover of Sahel rangelands (Gourma, Mali). Agric for Meteorol 198–199:155–167.

Olsoy PJ, Mitchell JJ, Levia DF et al (2016) Estimation of big sagebrush leaf area index with terrestrial laser scanning. Ecol Ind 61:815–821.

Pan N, Wang S, Wei F et al (2021) Inconsistent changes in NPP and LAI determined from the parabolic LAI versus NPP relationship. Ecol Ind 131:108134.

Park JY, Muller-Landau HC, Lichstein JW et al (2019) Quantifying leaf phenology of individual trees and species in a tropical forest using unmanned aerial vehicle (UAV) images. Remote Sens 11:1534.

Peng X, Han W, Ao J, Wang Y (2021) Assimilation of LAI derived from UAV multispectral data into the SAFY model to estimate maize yield. Remote Sens 13:1094.

Prăvălie R (2016) Drylands extent and environmental issues. A Global Approach Earth-Sci Rev 161:259–278.

Roser A, Enterkine J, Requena-Mullor JM et al (2022) Drone imagery protocols to map vegetation are transferable between dryland sites across an elevational gradient. Ecosphere 13:e4330.

Ryu Y, Baldocchi DD, Kobayashi H et al (2011) Integration of MODIS land and atmosphere products with a coupled-process model to estimate gross primary productivity and evapotranspiration from 1 km to global scales: GLOBAL GPP AND ET. Global Biogeochem Cycles. https://doi.org/10.1029/2011gb004053

Sha Z, Wang Y, Bai Y et al (2019) Comparison of leaf area index inversion for grassland vegetation through remotely sensed spectra by unmanned aerial vehicle and field-based spectroradiometer. J Plant Ecol 12:395–408.

Smith WK, Dannenberg MP, Yan D et al (2019) Remote sensing of dryland ecosystem structure and function: progress, challenges, and opportunities. Remote Sens Environ 233:111401.

Taylor SD, Browning DM, Baca RA, Gao F (2021) Constraints and opportunities for detecting land surface phenology in Drylands. J Remote Sens. https://doi.org/10.34133/2021/9859103

Tian J, Wang L, Li X et al (2017) Comparison of UAV and WorldView-2 imagery for mapping leaf area index of mangrove forest. Int J Appl Earth Obs Geoinf 61:22–31.

Wang J, Xiao X, Bajgain R et al (2019) Estimating leaf area index and aboveground biomass of grazing pastures using Sentinel-1, Sentinel-2 and Landsat images. ISPRS J Photogramm Remote Sens 154:189–201.

Wang W, Gao X, Cheng Y et al (2022) QTL mapping of leaf area index and chlorophyll content based on UAV remote sensing in wheat. Agriculture 12:595.

Wittstruck L, Jarmer T, Trautz D, Waske B (2022) Estimating LAI from winter wheat using UAV data and CNNs. IEEE Geosci Remote Sens Lett 19:1–5.

Wood DJA, Preston TM, Powell S, Stoy PC (2022) Multiple UAV flights across the growing season can characterize fine scale phenological heterogeneity within and among vegetation functional groups. Remote Sens 14:1290.

Zhang Y, Ta N, Guo S et al (2022) Combining spectral and textural information from UAV RGB images for leaf area index monitoring in kiwifruit orchard. Remote Sens 14:1063.